# Many-body instability of Coulomb interacting bilayer graphene: RG approach

Oskar Vafek[1] and Kun Yang[1]

[1]*National High Magnetic Field Laboratory and Department of Physics, Florida State University, Tallahassee, Florida 32306, USA*

(Dated: June 15, 2009)

Low-energy electronic structure of (unbiased) bilayer graphene is made of two Fermi points with *quadratic* dispersions, if trigonal-warping and other high order contributions are ignored. We show that as a result of this qualitative difference from single-layer graphene, short-range (or screened Coulomb) interactions are marginally *relevant*. We use renormalization group to study their effects on low-energy properties of the system, and show that the two quadratic Fermi points spontaneously split into four Dirac points, at zero temperature. This results in a nematic state that spontaneously breaks the six-fold lattice rotation symmetry (combined with layer permutation) down to a two-fold one, with a finite transition temperature. Critical properties of the transition and effects of trigonal warping are also discussed.

The ability to predict the nature of the low temperature state of an interacting quantum system is one of the main goals of condensed matter theory. Nevertheless, despite ongoing effort, no single method has proved universally sufficient and experimental input is essentially inevitable.

Under special circumstances, however, progress can be made. In particular, in non-interacting systems with susceptibilities diverging as the temperature approaches zero, the inclusion of arbitrarily small interaction can be shown to lead to a finite, but also arbitrarily small transition temperature. The method of choice in this case is the renormalization group (RG), which has the virtue of unbiased determination of the leading instability[1].

In this paper we apply the RG method to the bilayer graphene with Bernal stacking[2,3,4,5]. While in general, the motion of the non-interacting electrons in such potential does not lead to diverging susceptibilities since the energy spectrum has two sets of four Dirac points in the corners of the Brillouin zone (due to trigonal warping)[3,4], if only nearest neighbor hopping is considered each set of four Dirac points merges into a single degenerate point with parabolic dispersion (See Fig. 1). As the nearest neighbor hopping amplitudes are the largest, the latter is the natural starting point of theoretical analysis[6,7].

We start with the tight-binding Hamiltonian for electrons hopping on the bilayer honeycomb lattice with Bernal stacking

$$\mathcal{H}=\sum_{\langle \mathbf{r}\mathbf{r}'\rangle}\left[t_{\mathbf{r}\mathbf{r}'}c^{\dagger}_{\sigma}(\mathbf{r})c_{\sigma}(\mathbf{r}')+h.c.\right]+\frac{1}{2}\sum_{\mathbf{r}\mathbf{r}'}\delta\hat{n}(\mathbf{r})V(\mathbf{r}-\mathbf{r}')\delta\hat{n}(\mathbf{r}'), \tag{1}$$

where, in the nearest neighbor approximation, the (real) hopping amplitudes $t$ connect the in-plane nearest neighbor sites belonging to different sublattices and, for one of the sublattices, also the sites vertically above it with amplitude $t_\perp$. Since there are four sites in the unit cell, there are four bands whose dispersion for the above model

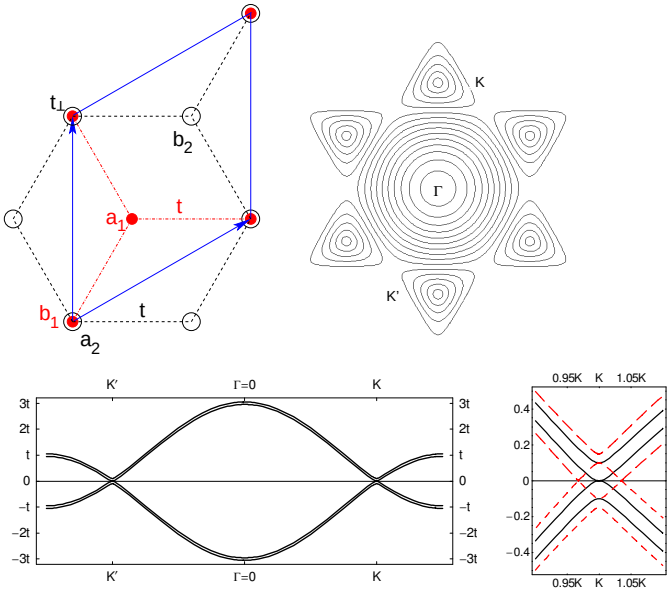


FIG. 1: (Upper left) Honeycomb bilayer unit cell. Atoms in the lower layer (2) are marked as empty (black) circles, atoms in the upper layer (1) are filled (red) circles. As a starting point, only the intralayer nearest neighbor hopping amplitudes $t$ and the interlayer hopping amplitudes $t_\perp$ are considered. (Upper right) Constant energy contours of the resulting dispersion, with minima at $K=\frac{4\pi}{\sqrt{3}3a}\hat{y}$ and $K'$ points and maximum at $\Gamma$ point. (Lower left) The energy dispersion of the four bands along the vertical cut in the Brillouin zone. The band splitting at the $K$ (and $K'$) points is $t_\perp$. (Lower right) Magnification of the dispersion (in units of $t$) near the degeneracy point (solid black) as well as the dispersion in the nematic state (dashed red) with $\Delta_x\neq 0$ (See Eq.19).

comes from the solution of the eigenvalue problem:

$$\begin{bmatrix} 0 & d^*_{\mathbf{k}} & t_\perp & 0\\ d_{\mathbf{k}} & 0 & 0 & 0\\ t_\perp & 0 & 0 & d_{\mathbf{k}}\\ 0 & 0 & d^*_{\mathbf{k}} & 0\end{bmatrix}\begin{bmatrix} b_1(\mathbf{k})\\ a_1(\mathbf{k})\\ a_2(\mathbf{k})\\ b_2(\mathbf{k})\end{bmatrix}=E(\mathbf{k})\begin{bmatrix} b_1(\mathbf{k})\\ a_1(\mathbf{k})\\ a_2(\mathbf{k})\\ b_2(\mathbf{k})\end{bmatrix}. \tag{2}$$

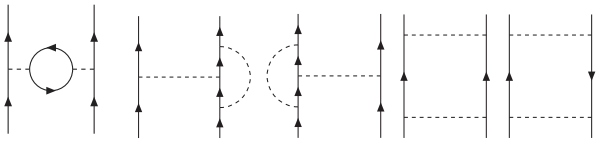

FIG. 2: Diagrams appearing at 1-loop RG. The vertices are either $\delta_{\alpha\beta}$ or $\Sigma^{\mu}_{\alpha\beta}$.

We find $E(\mathbf{k}) = \pm\left(\frac{1}{2}t_\perp \pm \sqrt{|d_\mathbf{k}|^2 + \frac{1}{4}t_\perp^2}\right)$, with $d_\mathbf{k} = t\left[2\cos\left(\frac{\sqrt{3}}{2}k_y a\right)e^{-\frac{i}{2}k_x a} + e^{ik_x a}\right]$. Two of the bands are gapped (at $\mathbf{K}, \mathbf{K}'$ by $t_\perp$) and become separated from the low energy pair which touches at $\mathbf{k} = 0$ (See Fig.1). The resulting density of states at zero energy is therefore finite.

The repulsive interaction $V(\mathbf{r}-\mathbf{r}')$ in Eq.(1) is taken to have a finite range $\xi$ which is however much larger than the lattice spacing $a$. This is assumed to be the correct starting point, since the full Coulomb interactions is screened[8] at low energy due to the finite density of states. The analysis starting from the $1/|\mathbf{r}-\mathbf{r}'|$ interaction will be postponed to a future publication.

Following Nilsson *et. al.*[9] we project out the gapped bands. The resulting low energy effective (imaginary time) action (which includes both $K$ and $K'$ valleys) is

$$\begin{aligned}\mathcal{S} &= \int d\tau d^2\mathbf{r}\left[\psi^\dagger\left(\frac{\partial}{\partial\tau} + \sum_{a=x,y}\Sigma^a d^a_\mathbf{p}\psi\right)\right] \\ &+ \frac{1}{2}g_1\int d\tau d^2\mathbf{r}\psi^\dagger\psi(\mathbf{r},\tau)\psi^\dagger\psi(\mathbf{r},\tau) \\ &+ \frac{1}{2}g_2\int d\tau d^2\mathbf{r}\psi^\dagger\Sigma^z\psi(\mathbf{r},\tau)\psi^\dagger\Sigma^z\psi(\mathbf{r},\tau) \\ &+ \frac{1}{2}g_3\int d\tau d^2\mathbf{r}\sum_{a=x,y}\psi^\dagger\Sigma^a\psi(\mathbf{r},\tau)\psi^\dagger\Sigma^a\psi(\mathbf{r},\tau) \quad (3)\end{aligned}$$

where the four component Fermi (Grassman) fields

$$\psi(\mathbf{r},\tau) = \int_0^\Lambda \frac{d^2\mathbf{k}}{(2\pi)^2}e^{i\mathbf{k}\cdot\mathbf{r}}\begin{bmatrix} a_1(\mathbf{K}+\mathbf{k},\tau) \\ b_2(\mathbf{K}+\mathbf{k},\tau) \\ a_1(\mathbf{K}'+\mathbf{k},\tau) \\ b_2(\mathbf{K}'+\mathbf{k},\tau)\end{bmatrix} \quad (4)$$

and

$$\begin{aligned} d^x_\mathbf{k} &= \frac{k_x^2-k_y^2}{2m}, \quad d^y_\mathbf{k} = \frac{2k_xk_y}{2m}, & (5)\\ \Sigma^x &= 1\sigma^x, \ \ \Sigma^y = \tau^z\sigma^y, \ \ \Sigma^z = \tau^z\sigma^z. & (6)\end{aligned}$$

The Pauli matrices $\sigma_j$ act on the layer indices 1-2 and the $\tau$ matrices act on the valley indices $\mathbf{K}$-$\mathbf{K}'$. The effective mass is $m = 2t_\perp/(9t^2)$, and $\psi$ represents $\frac{N}{2}-$copies of the four component pseudo-spinor. $N = 4$ for spin 1/2, and e.g. for $s = 1,\dots N$, $\psi^\dagger\Sigma^z\psi(\mathbf{r},\tau) = \psi^\dagger_{\alpha s}\Sigma^z_{\alpha\beta}\psi_{\beta s}$. Note that $\Sigma's$ have the same multiplication table as the Pauli $\sigma's$: $\Sigma^\mu\Sigma^\nu = 1_4\delta_{\mu\nu} + i\epsilon_{\mu\nu\lambda}\Sigma^\lambda$ and are traceless, too. $\Lambda$ is a momentum cutoff which restricts the modes to the vicinity of the $\mathbf{K}$-$\mathbf{K}'$ points and whose order of magnitude is $\lesssim\sqrt{2mt_\perp}$.

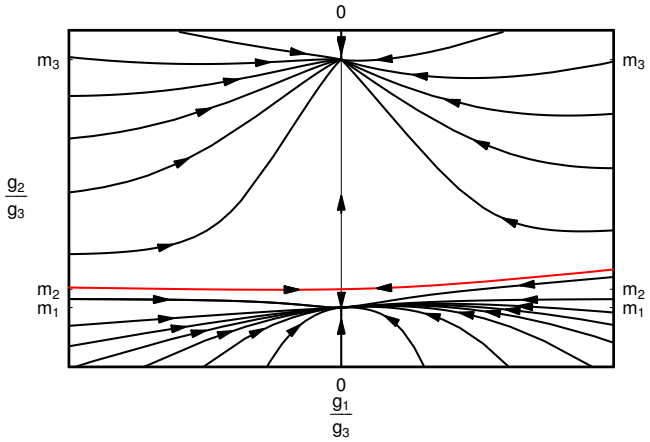


FIG. 3: RG flow diagram of the ratios $g_1/g_3$ and $g_2/g_3$ for $g_3 < 0$. While the ratio $g_1/g_3$ flows to zero (even if the starting point is $g_2 = g_3 = 0$ and $g_1 \neq 0$), the ratio $g_2/g_3$ flows to a fixed value, indicating two stable and one unstable rays with slopes $m_1 \approx -0.525$, $m_3 \approx 13.98$ and $m_2 \approx 0.545$, respectively.

The coupling constant $g_1 = \int d^2\mathbf{r}V(\mathbf{r})$, i.e. it is the $\mathbf{q} = 0$ Fourier component of $V(\mathbf{r})$. The coupling constants $g_2$ and $g_3$ are zero in the starting action, but as will be shown next, they get generated in the momentum-shell RG[1], and therefore they are made explicit in the original action.

From simple power-counting, the (engineering) scaling dimension of the field $\psi$ is $L^{-1}$ and $L^2$ for $\tau$. This makes $g_1$, $g_2$ and $g_3$ marginal (at the tree-level) and the question is how they flow upon inclusion of the loop corrections. To answer this we note that all possible Wick contractions[1] of four-fermion operators correspond to the diagrams in the Figure (2). The RG equations obtained by integrating fermion modes within a thin shell $\Lambda$ and $\Lambda/s$ (centered at the $K$ point), and $\int_{-\infty}^{\infty}\frac{d\omega}{2\pi}$, are:

$$\begin{aligned}\frac{dg_1}{d\ln s} &= \left[-4g_1g_3\right]\frac{m}{4\pi} & (7)\\ \frac{dg_2}{d\ln s} &= \left[-4(N-1)g_2^2 + 4g_3^2 + 4g_1g_2 - 12g_2g_3\right]\frac{m}{4\pi} & (8)\\ \frac{dg_3}{d\ln s} &= \left[-(g_1-g_3)^2 - (g_2-g_3)^2 - 2(N+1)g_3^2\right]\frac{m}{4\pi} & (9)\end{aligned}$$

While the above equations cannot be solved in a closed form, it is possible to fully analyze the qualitative nature of the RG flows. Such analysis is facilitated by the observation that

$$\frac{dg_3}{d\ln s} \leq 0$$

| $\psi^\dagger\tau^\mu\sigma^\nu\psi$ | $\nu=0$ | $\nu=x$ | $\nu=y$ | $\nu=z$ |
|---|---|---|---|---|
| $\mu=0$ | $0,0,0$ | $1,-1,-2N$ | $1,-1,0$ | $2,2,-4$ |
| $\mu=x$ | $1,-1,0$ | $0,0,0$ | $2,2,-4$ | $1,-1,0$ |
| $\mu=y$ | $1,-1,0$ | $0,0,0$ | $2,2,-4$ | $1,-1,0$ |
| $\mu=z$ | $0,0,0$ | $1,-1,0$ | $1,-1,-2N$ | $2,2-4N,-4$ |

TABLE I: The susceptibility coefficients $A, B, C$ in Eq.(17) for different particle-hole order parameters $\psi^\dagger\mathcal{O}_i\psi$. In the physical case $N=4$.

| $\psi_{\alpha s}(\tau^\mu\sigma^\nu)_{\alpha\beta}\psi_{\beta s'}$ | $\nu=0$ | $\nu=x$ | $\nu=y$ | $\nu=z$ |
|---|---|---|---|---|
| $\mu=0$ | $-1,-1,0$ | $-2,2,-4$ | $0,0,0$ | $-1,-1,0$ |
| $\mu=x$ | $-2,2,-4$ | $-1,-1,0$ | $-1,-1,0$ | $0,0,0$ |
| $\mu=y$ | $-2,2,-4$ | $-1,-1,0$ | $-1,-1,0$ | $0,0,0$ |
| $\mu=z$ | $-1,-1,0$ | $-2,2,-4$ | $0,0,0$ | $-1,-1,0$ |

TABLE II: The susceptibility coefficients $A', B', C'$ in Eq.(18) for different particle-particle order parameters $\psi_{\alpha\sigma}\mathcal{O}^{(i)}_{\alpha\beta}\psi_{\beta\sigma'}$.

which means that, unless $g_1 = g_2 = g_3 = 0$ when the equality holds, $g_3$ strictly decreases under RG rescaling. We can therefore trade the parametric dependence on $s$ of $g_1$ and $g_2$ for their dependence on $g_3$ *and* retain the direction of the RG flow. For $g_3 < 0$ ($> 0$), an increase in $d\log s$ therefore corresponds to an increase (decrease) in $\frac{dg_3}{g_3}$. Since the system is autonomous, we can eliminate $\log s$ and arrive at a system

$$\frac{dg_1}{dg_3} = f\left(\frac{g_1}{g_3}, \frac{g_2}{g_3}\right) \tag{10}$$

$$\frac{dg_2}{dg_3} = g\left(\frac{g_1}{g_3}, \frac{g_2}{g_3}\right) \tag{11}$$

where

$$f(x,y) = \frac{-4x}{-x^2-y^2-2(N+2)+2x+2y} \tag{12}$$

$$g(x,y) = \frac{-4(N-1)y^2+4+4xy-12y}{-x^2-y^2-2(N+2)+2x+2y} \tag{13}$$

The system of Eqs.(10)-(11) is in turn homogeneous and can therefore be written as

$$g_3\frac{d\frac{g_1}{g_3}}{dg_3} = -\frac{g_1}{g_3} + f\left(\frac{g_1}{g_3}, \frac{g_2}{g_3}\right) \tag{14}$$

$$g_3\frac{d\frac{g_2}{g_3}}{dg_3} = -\frac{g_2}{g_3} + g\left(\frac{g_1}{g_3}, \frac{g_2}{g_3}\right). \tag{15}$$

The above system has three fixed points, all of which have $g_1/g_3 = 0$, while $g_2/g_3 = m_1, m_2, m_3$. As shown in the Fig.(3), $m_1 \approx -0.525$ and $m_3 \approx 13.98$ are sinks, while $m_2 \approx 0.545$ has one attractive direction and one repulsive. This means that once $g_3$ gets to be negative, only $g_2$ and $g_3$ become important (their ratio being fixed) while $g_1$ is too small compared to $g_3$. To see that this is indeed what happens if the starting point is $g_1(s=1) > 0$ and $g_2(s=1) = g_3(s=1) = 0$, note that the Eqs.(7-9) imply that finite $g_1$ generates finite and negative $g_3$ upon first iteration while $g_2$ remains zero until the second iteration. This means that we start with $g_1/g_3 \to -\infty$ and $g_2/g_3 = 0$ which is *below* the (red) separatrix, thus the flow is into the region of attraction of $m_1$ (Fig.(3)).

From Eqs.(7-9) we see for the fixed ratios $g_1/g_3 = 0$ and $g_2/g_3 = m_j$, $g_3$ becomes large and negative, indicating a runaway flow. Given the flow of the coupling

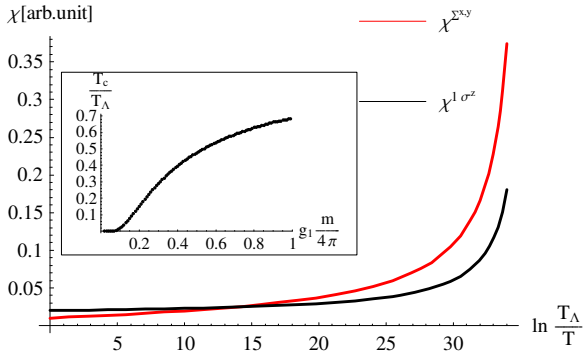


FIG. 4: Numerical integration of the susceptibilities in Eq.(17) for $g_1(s=1) = 0.01$ and $g_2(s=1) = g_3(s=1) = 0$. The strongest divergence is towards the nematic order. (Inset) Numerically determined nematic transition temperature in units of cutoff $T_\Lambda \lesssim t_\perp$ as a function of the dimensionless coupling $g_1\frac{m}{4\pi}$.

constants we can determine the susceptibilities towards the formation of ordered states. In particular, we consider coupling the fermions to external sources, which correspond to the possible broken symmetry states. We therefore have additional terms in the action:

$$\begin{aligned}\Delta\mathcal{S} &= -\Delta^{\mathcal{O}_i}_{ph}\int d\tau d^2\mathbf{r}\psi^\dagger\mathcal{O}_i\psi(\mathbf{r},\tau) \\ &- \Delta^{\mathcal{O}_i}_{pp}\int d\tau d^2\mathbf{r}\psi_{\alpha\sigma}\mathcal{O}^i_{\alpha\beta}\psi_{\beta\sigma'}(\mathbf{r},\tau)\end{aligned} \tag{16}$$

Such terms, with infinitesimal $\Delta$'s explicitly break the symmetry and so are relevant operators. The question of instability is answered by finding the renormalization of the vertices[10]. The one which diverges first determines the broken symmetry states. After a straigthforward calculation we find that for a general particle-hole order parameter $\mathcal{O}_i = \tau^\mu\sigma^\nu$ where $\mu,\nu = 0,1,2,3$ and $\tau_0 = \sigma_0 = 1$,

$$\Delta^{\tau^\mu\sigma^\nu}_{ph,ren} = \Delta^{\tau^\mu\sigma^\nu}_{ph}\left(1 + [Ag_1 + Bg_2 + Cg_3]\frac{m}{4\pi}\ln s\right) \tag{17}$$

where the coefficients $A$, $B$, and $C$ are given in the Table I. Similarly, for a general particle-particle order parame-

ter $\psi_{\alpha\sigma}\mathcal{O}^{(i)}_{\alpha\beta}\psi_{\beta\sigma'}$

$$\Delta^{\tau^\mu\sigma^\nu}_{pp,ren} \;=\; \Delta^{\tau^\mu\sigma^\nu}_{pp}\left(1+[A'g_1+B'g_2+C'g_3]\,\frac{m}{4\pi}\ln s\right) \tag{18}$$

where the coefficients $A'$, $B'$, and $C'$ are given in the Table II.

The instability towards a particular order occurs at an energy scale (*i.e.* temperature) at which the corresponding coefficient of the $\ln s$ in Eqs.(17-18) diverges. Since $N=4$ and the fixed point value of $g_2/g_3\approx -0.525$, with $g_3$ large and negative, it can be seen from Table I that the instability appears in the $\Sigma^{x,y}$ channel, which as we discuss next corresponds to a *nematic* order. The numerical integration of the RG equations (7-9) starting with $g_1(s=1)>0$ and $g_2(s=1)=g_3(s=1)=0$ shown in Fig.(4) indeed confirms that the susceptibility diverges fastest in this channel. Within the continuum model and in weak coupling, the instability is therefore towards the order parameter, which we can parametrize by a complex field

$$\Delta_{nem}(\mathbf{r})\equiv\Delta_x(\mathbf{r})+i\Delta_y(\mathbf{r})=\langle\psi^\dagger(\mathbf{r})\,(\Sigma^x+i\Sigma^y)\,\psi(\mathbf{r})\rangle.$$

To see that this is indeed a nematic order, note that at $\mathbf{q}=0$ (1) it is translationally invariant and (2) even under rotations by $\pi$. In fact, as the low energy Hamitonian is invariant under arbitrary rotations by an angle $\alpha$, i.e. $U^\dagger(\alpha)\mathcal{H}U(\alpha)=\mathcal{H}$, where $U_\alpha=e^{-i\alpha\hat{L}_z}e^{-i\alpha\Sigma^z}$, $L_z=x\frac{\partial}{\partial y}-y\frac{\partial}{\partial x}$, we find that under a rotation by $\alpha$

$$\Delta_{nem}(\mathbf{r})\to\Delta_{nem}(\mathbf{r})e^{2i\alpha}.$$

This shows that the order parameter is even under rotations by $\pi$ and odd under rotations by $\pi/2$, which makes it nematic. For uniform $\Delta_{nem}(\mathbf{r})$ the quadratic degeneracy point is split into two (massless) Dirac points by an amount proportional to the magnitude of the order parameter and the direction given by the nematic director.

The presence of the underlaying lattice further breaks the full rotational symmetry of the long distance effective Hamiltonian down to hexagonal symmetry centered on $a_2-b_1$ site, where the standard operations of $C_{6v}$ must be accompanied by the appropriate layer permutations. The two components of the order parameter, which give finite expectation values of, for instance, $\Delta_x(\mathbf{r})=$

$$\left\langle a^\dagger_{1\sigma}(\mathbf{r})\left(b_{2\sigma}(\mathbf{r}-a\hat{x})-\frac{1}{2}\sum_{s=\pm}b_{2\sigma}(\mathbf{r}+\frac{a}{2}\hat{x}s\frac{\sqrt{3}}{2}\hat{y})\right)+h.c.\right\rangle \tag{19}$$

and $\Delta_y(\mathbf{r})=$

$$\left\langle a^\dagger_{1\sigma}(\mathbf{r})\left(\frac{\sqrt{3}}{2}\sum_{s=\pm}sb_{2\sigma}(\mathbf{r}+\frac{a}{2}\hat{x}+s\frac{\sqrt{3}}{2}\hat{y})\right)+h.c.\right\rangle \tag{20}$$

form a two dimensional representation of the hexagonal group. Note that the nematic order parameter remains even under $\pi$-rotation followed by the layer permutation.

From the arguments above we expect that the lattice has an important effect on the critical nature of the phase transition, which would otherwise be of Kosterlitz-Thousless kind. The reason is the existence of the third order invariant $\Delta_x^3-3\Delta_x\Delta_y^2$. As a result the finite temperature phase transition should be described by the effective Hamiltonian

$$\mathcal{H}_{nem}=\sum_{\langle\mathbf{x}\mathbf{x}'\rangle}-J\cos[2(\theta(\mathbf{x})-\theta(\mathbf{x}'))]+h\sum_{\mathbf{x}}\cos[6\theta(\mathbf{x})] \tag{21}$$

where $\Delta_x(\mathbf{x})+i\Delta_y(\mathbf{x})=e^{2i\theta(\mathbf{x})}$, $\theta\in(0,2\pi]$ and the sum runs over the vertices of the triangular sub-lattice spanned by $a_1$ sites. This corresponds to the $p=3$ case of the two dimensional planar model studied by Jose et.al.[11] and the concomitant absence of the Gaussian spin-wave phase. Instead there is a continuous transition between the low temperature phase where the director locks into one of three values and a high temperature phase where vortices unbind. Such transition is believed to belong to the 2D three-state Potts model universality class[12] with exponents[13] $\nu=5/6$ and $\eta=4/15$.

Finally, we discuss the effects of the trigonal warping which splits each of the quadratic degeneracies into four massless Dirac points, which were ignored up to now. If we denote the energy scale associated with such terms as $T_{trig}$, below which the dispersion must be modified, then the transition will still occur provided that the mean-field transition temperature $T_c$ estimated from the above model and plotted in the inset of Fig.(4) satisfies $T_c\gg T_{trig}$. For screened Coulomb interactions[8] $g_1\frac{m}{4\pi}\sim\mathcal{O}(1)$, leading to $T_c\lesssim t_\perp$. Since the current estimates of $T_{trig}$ are of the same order of magnitude[14], the ultimate test is experimental.

Acknowledgements: While this paper was in preparation, we became aware of Ref.[15] where lattices with fourfold and sixfold rotational symmetry are constructed in either case the parabolic degeneracy points are protected by the point group symmetry. In there, the degeneracy point maps unto itself under time reversal, unlike our $K$ and $K'$, and nematic was found to be stabilized (within mean-field) only at finite coupling. This work is supported in part by NSF grant No. DMR-0704133 (KY). Part of this work was carried out while the authors were visiting Kavli Institute for Theoretical Physics (KITP). The work at KITP is supported in part by NSF grant No. PHY-0551164.

[1] R. Shankar, Rev. Mod. Phys. **66**, 129 (1994).

[2] K. S. Novoselov, E. McCann, S. V. Morozov, V. I. Fal'ko, M. I. Katsnelson, U. Zeitler, D. Jiang, F. Schedin, and A. K. Geim, Nature Physics **2**, 177 (2006).

[3] E. McCann and V. I. Fal'ko, Physical Review Letters **96**, 086805 (2006).

[4] A. H. C. Neto, F. Guinea, N. M. R. Peres, K. S. Novoselov, and A. K. Geim, Reviews of Modern Physics **81**, 109 (2009).

[5] A. K. Geim and A. H. MacDonald, Physics Today **60**, 35 (2007).

[6] J. Nilsson, A. H. C. Neto, N. M. R. Peres, and F. Guinea, Physical Review B **73**, 214418 (2006).

[7] H. Min, G. Borghi, M. Polini, and A. H. MacDonald, Physical Review B **77**, 041407 (2008).

[8] E. H. Hwang and S. D. Sarma, Physical Review Letters **101**, 156802 (2008).

[9] J. Nilsson, A. H. C. Neto, F. Guinea, and N. M. R. Peres, Physical Review B **78**, 045405 (2008).

[10] A. V. Chubukov (2009), arXiv:0902.4188.

[11] J. V. José, L. P. Kadanoff, S. Kirkpatrick, and D. R. Nelson, Phys. Rev. B **16**, 1217 (1977).

[12] D. R. Nelson, *Defects and Geometry in Condensed Matter Physics* (Cambridge University Press, Cambridge, UK, 2002), p.56.

[13] F. Y. Wu, Rev. Mod. Phys. **54**, 235 (1982).

[14] L. M. Zhang, Z. Q. Li, D. N. Basov, M. M. Fogler, Z. Hao, and M. C. Martin, Physical Review B **78**, 235408 (2008).

[15] K. Sun, H. Yao, E. Fradkin, and S. A. Kivelson (2009), arXiv:0905.0907.